Short Communication

A bio-tribocorrosion comparison between additively manufactured and forged Ti6Al4V parts

Sina Matin [a], Sahar Toorandaz [b], Saman Nikpour [a], Hamidreza Abdolvand [c], Ehsan Toyserkani [b], Yolanda S. Hedberg [a,d,*]

[a] *Department of Chemistry, Western University, London, ON N6A 5B7, Canada*
[b] *Multi-Scale Additive Manufacturing Lab, Department of Mechanical and Mechatronics Engineering, University of Waterloo, Waterloo, ON N2L 3G1, Canada*
[c] *Department of Mechanical and Materials Engineering, Western University, London, ON N6A 5B7, Canada*
[d] *Surface Science Western, Western University, London, ON N6G 0J3, Canada*

ARTICLE INFO

ABSTRACT

Ti6Al4V has been used widely as a biomedical alloy and is increasingly manufactured by additive manufacturing due to customized shapes. As implant material, it is frequently exposed to both friction and corrosive environments. This study investigates the effect of the fabrication process (laser powder bed fusion and forging) on the tribocorrosion behavior of Ti6Al4V in various environments including diluted hydrochloric acid to simulate the acidic environment in a crevice (HCl), phosphate-buffered saline (pH 7.3) with 10 g/L bovine serum albumin (PBS+BSA), and PBS+BSA with 30 mM H_2O_2. While the presence of BSA hindered the repassivation (reforming of the protective passive surface oxide), the presence of H_2O_2 accelerated it. HCl resulted in a localized tribo-corrosion process. The highest plastic deformation rate was found in the PBS+BSA solution followed by HCl and PBS+BSA+H_2O_2. In addition, AM parts presented a higher microhardness and smaller grain sizes compared to forged materials. There was no influence of the manufacturing process on the coefficient of friction (COF) in HCl and PBS+BSA solutions, however, a significantly higher COF was found for forged samples in PBS+BSA+H_2O_2 than AM samples. Tribocorrosion was more extensive for forged than AM Ti6Al4V in all solutions.

1. Introduction

There is a continuous need for metallic implants capable of enduring chemical and mechanical stresses throughout their lifespan inside the body [1]. Accordingly, high corrosion resistance to body fluid, biocompatibility, and adequate mechanical characteristics such as strength, elastic modulus, fatigue, and wear resistance are crucial [2–4]. A titanium alloy with relatively low density and the aforementioned features could resemble bone in a way to stimulate bone osteointegration [5]. Three main classes of biomedical alloys widely utilized are titanium alloys, stainless steel, and cobalt-chromium-molybdenum alloys. Each material has its own advantages and disadvantages, which make them suitable for customized applications [1]. Titanium alloys have been considered to be the most biocompatible due to the formation of a thin passive oxide layer on their surface. They also possess excellent mechanical properties (most importantly a stiffness close to the natural bone) with various applications in dental, hip, knee, and spine implants [6,7].

There is a medical advantage of customized implant shapes, while additive manufacturing (AM), especially laser powder bed fusion (LPBF) is increasingly used for these implants and replacing traditional casting or forging methods [8].

Titanium alloys are not considered the most wear-resistant option, so they are often used for bone integration only. However, the alloy is exposed to micromotions, especially in the trunnion (taper) region of artificial hip implants [1]. Synergistic effects of mechanical damage, such as wear and corrosion, can lead to the breakdown of the passive film and ultimately affect the longevity and functionality of an implant. This phenomenon is generally known as tribocorrosion, which releases metal ions and wear particles from biomedical alloys into the surrounding environment and triggers the body's immune and inflammatory systems [9–11]. Runa et al. reported the presence of albumin, an abundant protein in the human body, could reduce the repassivation ability of titanium- 6 wt.% aluminum – 4 wt.% vanadium (Ti6Al4V) alloy due to the high electrical charge on the surface and its transfer to the solution.

Fig. 1. Additively manufactured Ti6Al4V specimens on the build plate fabricated by LPBF technique.

They showed the importance of protein on the tribocorrosion of Ti6Al4V for biomedical usage [12]. Gopal et al. indicated the importance of hydrogen peroxide (H_2O_2) as a representative of reactive oxygen species and albumin on the tribocorrosion behaviour of Ti6Al4V. The oxidizing nature of H_2O_2 increased the repassivation rate (it helped reform the passive, protective oxide). The amount of generated oxide patches was increased in the presence of H_2O_2 and albumin which acted as a lubricant and caused lower friction [13]. It was shown that albumin could promote debris adhering to the sliding surface. Also, under anodic conditions (applied/induced oxidative potential), the adhesion between the protein and released particles was very low, resulting in an increased rate of mechanical wear [14]. So far, no studies were performed to evaluate the effect of the fabrication process on the bio-tribocorrosion behavior of Ti6Al4V in various environments. In this research, the effect of the fabrication process on the bio-tribocorrosion behavior of Ti6Al4V was studied using electrochemical, tribological, and material characterization testing methods.

2. Experimental methodology

2.1. Sample fabrication and preparation

Additively manufactured (AM) and forged Ti6Al4V specimens were supplied by the Multi-Scale Additive Manufacturing Lab, Waterloo University, Canada, and Ionbond, Switzerland, respectively. Details on the composition of both AM and forged specimens and the heat treatment process on forged specimen are given in the supplementary information (Tables S1–S3). For AM materials, a commercially available Ti6Al4V powder from AP&C (a GE additive company) with the particle size distribution of D10 < 19.5 μm, D50 < 35.5 μm, and D90 < 51.3 μm were used to manufacture the LPBF parts. An EOS M290 LPBF machine (EOS GmbH, Krailling, Germany) was employed to print the cuboid parts ($3 \times 10 \times 10$ mm) with similar processing parameters (laser power of 150 W, laser velocity of 1250 mm/s, layer thickness of 0.02 mm and hatching spacing of 0.08 mm) using a rotated stripe scanning strategy. The selected parameters represent a volumetric energy density of 75 J/mm^3, wherein the volumetric energy density is defined as the ratio of laser power to the product of process speed, layer thickness, and hatch distance. Notably, this energy density value aligns with optimal ranges previously reported by various researchers [15,16]. It is important to note that there was no skin in the printed parts. AM electrodes were cut as square specimens with a $3 \times 10 \times 10$ mm dimension (Fig. 1)

and forged specimens were fabricated as disks with 22 mm diameter and 2 mm thickness. The forged specimens were annealed at 700–750 $^{\circ}$C and air-cooled in conformation with standards ASTM F136, ASTM B348/10 GRADE 5, and ISO5832–3. [17].

Ti6Al4V specimens were ground with a sequence of SiC papers (P600, P800, P1200, and P2500) to achieve the same surface condition for all specimens. Then, the samples were rinsed in type I water (resistivity = 18.2 MΩ cm), sonicated in ethanol and acetone (5 min each), and dried in a stream of Ar gas prior to an experiment.

2.2. Solution preparation

Solutions were prepared with American Chemical Society (ACS) reagent (pro analysis) grade hydrochloric acid - HCl (37.0%), phosphate buffered saline - PBS (8.77 g/L NaCl, 1.28 g/L Na_2HPO_4, and 1.36 g/L KH_2PO_4), bovine serum albumin (BSA, heat shock fraction, pH 7, ≥98%), and hydrogen peroxide - H_2O_2 (30% w/w) provided by Sigma-Aldrich using Type I water (18.2 MΩ cm) prepared using a Millipore Milli-Q Reference or plus system. Three different solutions were made including 0.1 M HCl (pH approximately 1.5), PBS + 10 g/L BSA, and PBS + 10 g/L BSA + 30 mM H_2O_2. The pH of the PBS + 10 g/L BSA, and PBS + 10 g/L BSA + 30 mM H_2O_2 solutions were adjusted to around 7.2–7.4 by adding 0.01 M NaOH solution.

These three solutions simulate the crevice environment in implants (low pH – HCl), normal physiological environment (presence of proteins, pH 7.3, PBS+BSA), and inflammatory conditions (presence of reactive oxygen species, pH 7.3, PBS+BSA+H_2O_2), respectively [5]. In this study, the chemical environment of the anodic site in crevice corrosion was simulated, not the geometrical environment. Mechanically assisted crevice corrosion (MACC) has been reported especially for the taper region in artificial hip joints and is the combination of corrosion and mechanical stress or micromotions [18] while tribocorrosion is the combination of wear and corrosion resulting from the mechanical action on the surface due to the friction between two surfaces in a corrosive environment [19].

2.3. Electrochemical cell, instrumentation, and procedure

All corrosion potential (E_{corr}) measurements (at open circuit) were performed in a conventional three-electrode electrochemical cell using a Ti6Al4V specimen as the working electrode (connected through a spring contact in a clamp cell), and an Ag/AgCl sat. KCl electrode (0.199 V vs. standard hydrogen electrode) as the reference electrode.
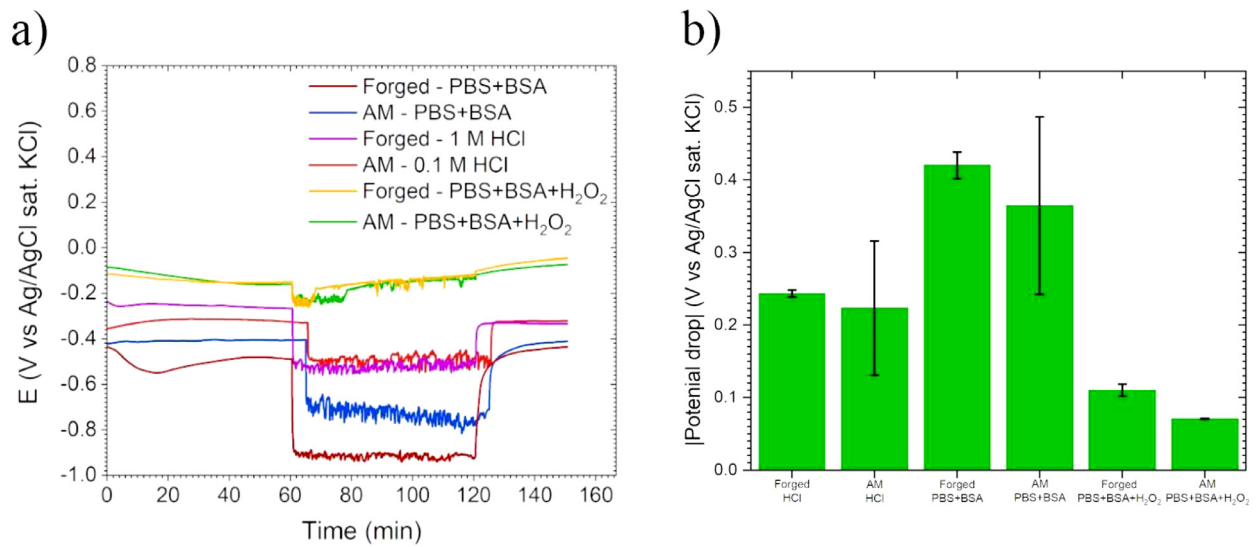
Fig. 2. (a) Representative curves of the corrosion potential of AM and forged Ti6Al4V in HCl (pH 1.5), PBS+BSA (pH 7.3), and PBS+BSA+H_2O_2 (pH 7.3) solutions at 37 °C. (b) Mean values of absolute potential drop from three measurements (error bars show the standard deviation between three independent measurements).
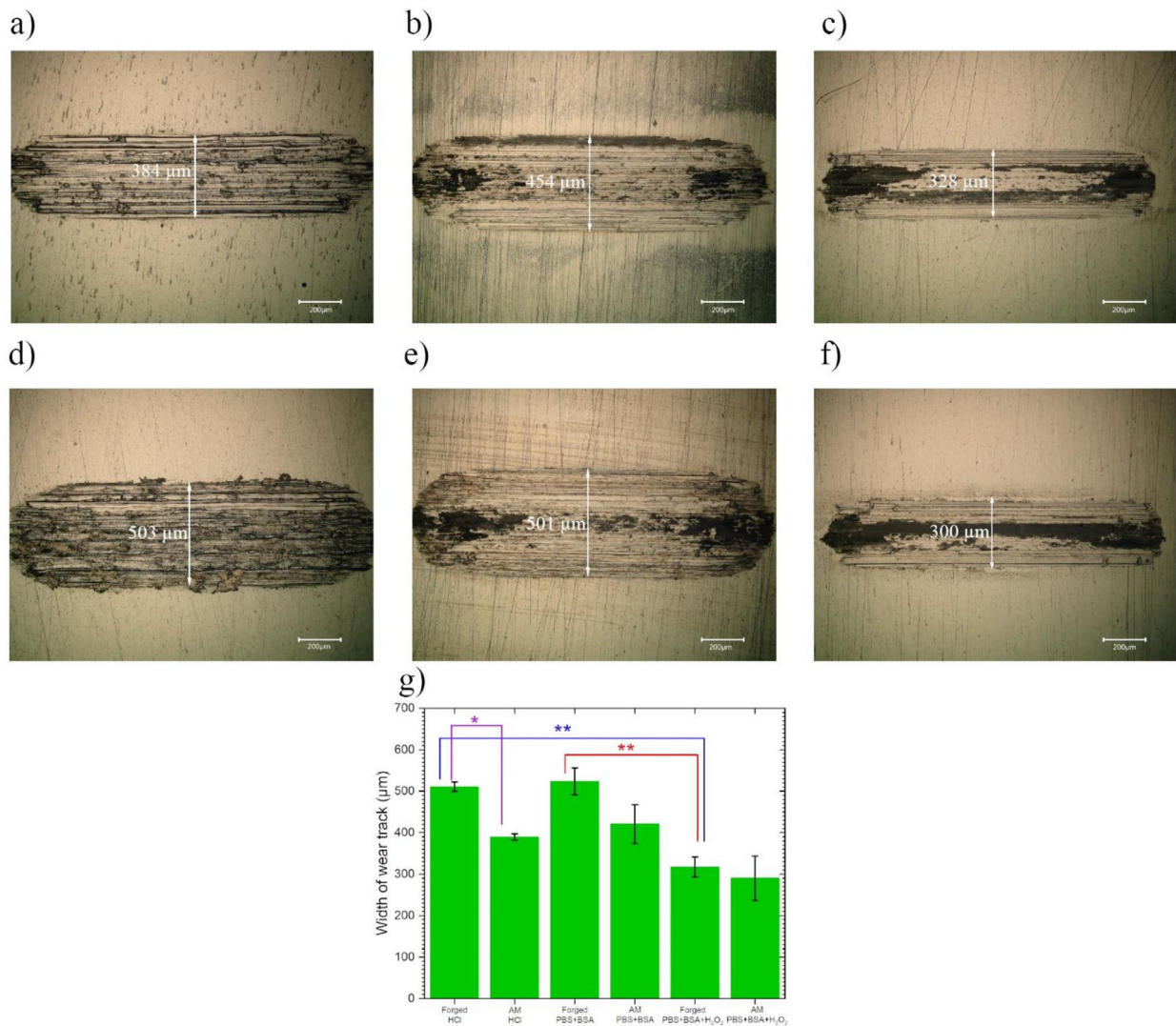
Fig. 3. Examples of wear track optical microscope images of AM (top) and forged (bottom) materials after tribocorrosion exposure to (a,d) HCl (pH 1.5), (b,e) PBS+BSA (pH 7.3), and (c,f) PBS+BSA+H_2O_2 (pH 7.3) solutions at 37 °C, g) * $p < 0.01$; ** - $p < 0.05$. * is for the fabrication process and ** is for solution.

2.4. Tribocorrosion

UMT TriboLab from Bruker was used in reciprocating (linear) ball-on-plate configuration to investigate the tribocorrosion of both AM and forged Ti6Al4V. The additively manufactured and forged specimens were used as a plate (18 × 18 × 3 mm) and disk (22 diameter × 2 mm thickness), respectively. A ceramic (Al_2O_3) ball with a diameter of 2 mm was allowed to slide against specimens at a speed of 1 mm/s and a stroke of 1.5 mm. All experiments were carried out with a load of 3 N and a duration of 7200 s. UMT TriboLab instrument was connected to ModuLab XM ECS Solartron potentiostat to measure the E_{corr} of specimens during the wear test. The specimens were immersed in 3 different solutions, as mentioned in the solution preparation section. The E_{corr} was measured before (60 min), during (60 min) and after the tribocorrosion test (30 min) by using a ModuLab XM ECS Solartron potentiostat. All tests were performed at 37± 1 ˚C. All specimens were in a sample holder with the same exposed surface area (1.5 cm² sealed by an O-ring).

2.5. Microhardness

The microhardness measurements of all samples were performed using Mitytoyo HM-200 with a load of 1 kg on ten different areas of the sample surface, and the average and standard deviation were reported.

2.6. Microscopy and electron backscatter diffraction (EBSD)

On completion of electrochemical experiments, the samples were rinsed with Type I water, dried in a low stream of Ar gas to avoid damage to oxide films, and stored in the vacuum desiccator for surface analysis. Keyence digital microscope VHX-6000 series was used to capture the wear track on the samples that were immersed in different solutions.

For imaging and measuring grain orientations using the electron backscatter diffraction (EBSD) technique, specimens were grinded up to 4000 grit size followed by 12 h vibratory polishing (Buehler VIBROMET 2) with a colloidal silica suspension. An Apreo-2 field emission gun scanning electron microscope (FEG-SEM) equipped with a high-resolution electron backscatter diffraction (EBSD) detector from Bruker was used. A 20 keV electron beam with 6.4 nA current was used and the sample was placed at the working distance of 18 mm. For collecting EBSD data, the sample-to-detector distance was set at 8 mm, and diffraction patterns were collected using the step size of 35 nm to resolve the fine microstructures of printed specimens.

3. Results and discussion

Fig. 2 shows the E_{corr} of AM and forged Ti6Al4V specimens in three different solutions including HCl, PBS+BSA, and PBS+BSA+H_2O_2 before, during, and after tribocorrosion tests performed on the AM and forged Ti6Al4V parts. The E_{corr} values stabilized during the 60 min without any friction. When the load was applied to the surface (after 60 min) and the ball started to slide on the surface, a sudden decrease in E_{corr} values was observed due to the removal of the oxide film and activation of the surface (increase of metal oxidation reactions) [20]. The amount of potential drop was highest in the PBS+BSA solution, followed by the HCl solution, and the PBS+BSA+H_2O_2 solution, which showed the lowest potential drop among all solutions. The load was finally released (after 120 min) and the E_{corr} values returned to approximately their initial values, which indicates a complete repassivation process (the oxide film is reformed). The E_{corr} of both AM and forged Al6Ti4V parts were most negative in PBS+BSA solutions due to (1) the cathodic inhibition by proteins [13,21,22], (2) no oxidation by H_2O_2 [17,23], and (3) the higher pH compared to HCl. The fluctuation was observed in all E_{corr} values during the fretting process (after 60 and before 120 min) due to the cyclic depassivation and repassivation phenomena [24]. In both HCl and PBS+BSA solutions, the E_{corr} remained stable with a small fluctuation which represents the dynamic equilibrium between depassivation
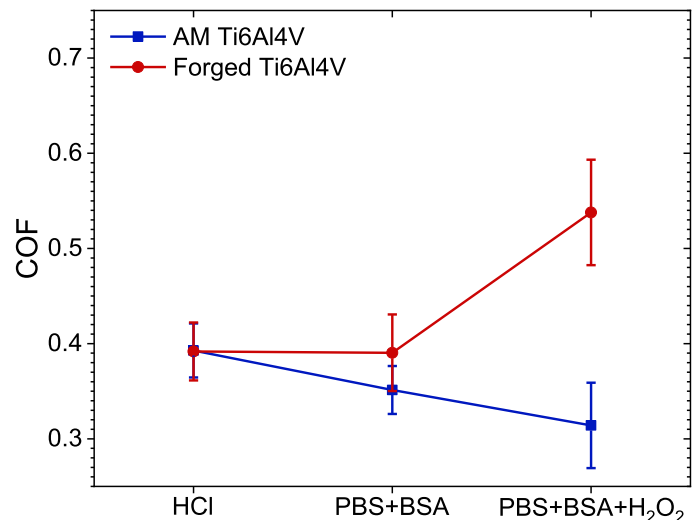
Fig. 4. Coefficient of friction (COF) of AM and forged Ti6Al4V during the fretting in HCl (pH 1.5), PBS+BSA (pH 7.3), and PBS+BSA+H_2O_2 (pH 7.3) solutions at 37 ˚C. The error bars show the standard deviation of independent triplicate measurements.

and repassivation. However, an interesting behavior was observed with the addition of H_2O_2 to the PBS+BSA solution. The potential dropped when the ceramic ball touched the surface and load was applied, but the potential started to increase instead of attaining equilibrium condition. This upward increase of potential during an active fretting process in the presence of H_2O_2 could have resulted from a higher repassivation rate compared to depassivation or the buildup of oxidative wear products, reducing the wear rate.

Fig. 3 represents the wear track of AM and forged alloys after tribocorrosion exposure to the three different solutions. A rougher appearance was observed in the worn surface area of the specimens in the acidic HCl solution (Fig. 3-a and d), along with localized corrosion in some areas [25]; however, no localized damage was observed in both BSA-containing solutions at pH 7.3. While localized corrosion of Ti6Al4V is not expected in 0.01 M HCl without friction, the disruption of the oxide film enables the direct exposure of the metal to the aggressive HCl environment. The width of the wear scar was smallest in the PBS+BSA+H_2O_2 solution (317±24.04 µm and 290±53.74 µm in forged and AM specimens, respectively) indicating less plastic deformation and abrasion followed by HCl (511±11.31 µm and 389.5 ± 7.78 µm in forged and AM specimen, respectively) and PBS+BSA (524±32.52 µm and 421±46.67 µm in forged and AM specimen, respectively) solutions. The coefficient of friction (COF) was measured for all specimens as shown in Fig. 4. The COF for both AM and forged parts was similar in the HCl and PBS+BSA solutions; however, the AM specimen showed significantly lower COF values in the PBS+BSA+H_2O_2 solution. The COF of the forged specimen in H_2O_2 containing solution was the highest among all specimens and conditions, Fig. 4. It is clear from Fig. 3-f that the wear track is relatively narrow in that solution and that the increased COF must hence be related to the wear products forming during the tribocorrosion process. We speculate that the larger average grain size of forged Ti6Al4V resulted in the formation of larger tribocorrosion debris in H_2O_2-containing solution which in turn led to a higher COF. To better understand that difference, we investigated the microhardness and microstructure differences of the AM and forged Ti6Al4V.

Fig. 5 demonstrates the microhardness values of both AM and forged Ti6Al4V parts. The microhardness was higher in the AM parts compared to the forged coupons, which could be due to the fabrication process and the difference in grain size. The crystallographic orientation (inverse pole figure along the x and z axes of the sample - IPFx and IPFz) and grain size of the AM and forged parts were measured using EBSD
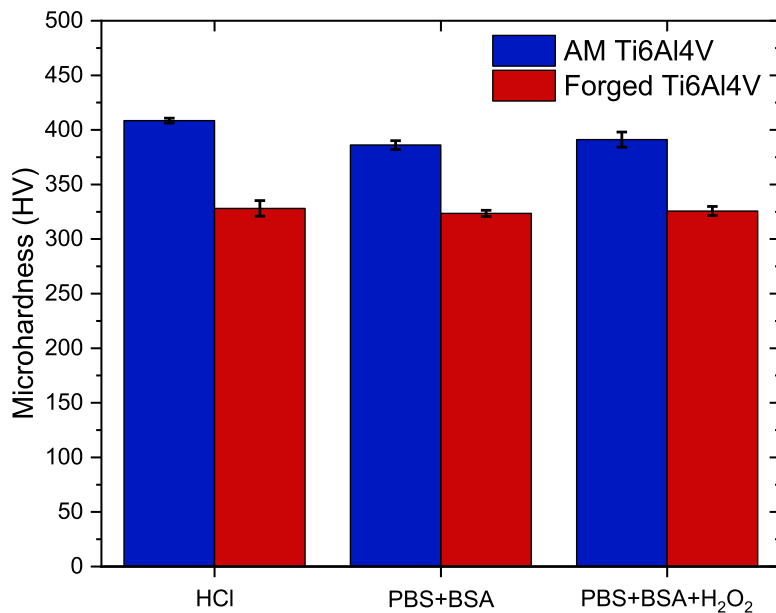
Fig. 5. Microhardness of AM and forged Ti6Al4V after the tribocorrosion exposure to HCl (pH 1.5), PBS+BSA (pH 7.3), and PBS+BSA+H_2O_2 (pH 7.3) solutions at 37 °C. The error bars show the standard deviation of ten measurements.
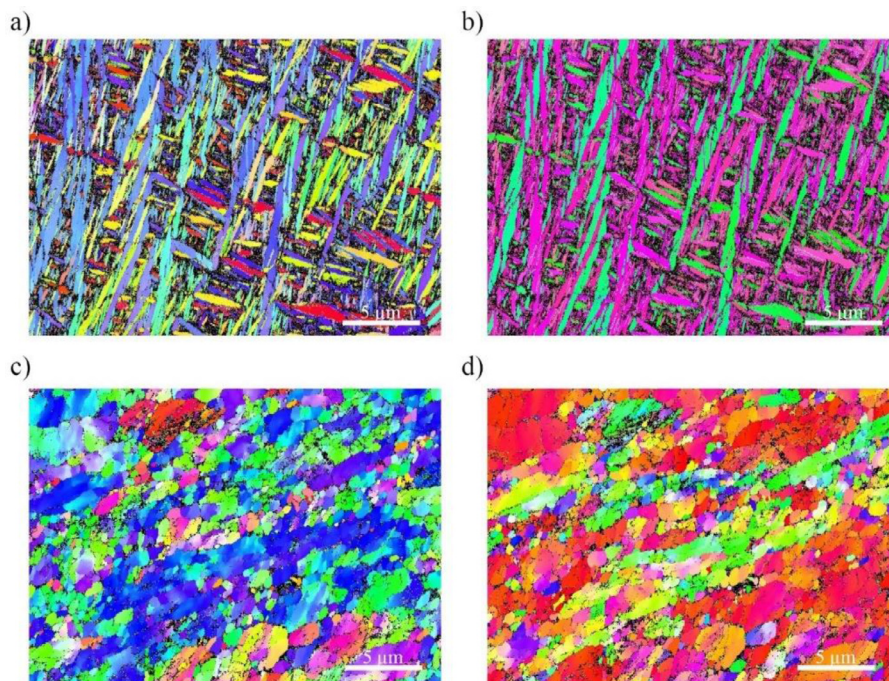
Fig. 6. Crystallographic orientation of Ti6Al4V, IPFx (a,c) and IPFz (b,d) of Ti6Al4V manufactured by AM (a,b) and by forging (c,d).

(Fig. 6). Elongated grain orientation was observed for the AM parts with an average grain size of 1.35 μm. The grain shape of the forged specimen was mixed of elongated and equiaxed grains with an average grain size of 2.07 μm. EBSD results were in good agreement with hardness data since smaller grain size in the AM parts resulted in higher microhardness. The comparison of COF data confirmed that there was no direct relationship between microhardness and COF in the HCl and PBS+BSA solutions. Buciumeanu et al. observed the same behavior and reported no correlation between the wear rate and hardness [20,26].

However, this study suggests that under oxidative wear and tribocorrosion conditions (in PBS+BSA+H_2O_2), the grain size and microhardness may play a role. While both AM and forged Ti6Al4V parts were repassivating quickly under those conditions, the oxidative wear buildup of the forged part resulted in more friction, possibly due to a larger grain size and larger wear debris. Future studies should investi-

gate whether the release of wear debris to a physiological environment is also dependent on the manufacturing type under those conditions.

4. Conclusions

Tribocorrosion behavior of AM and forged Ti6Al4V alloy was investigated in simulated physiological conditions (crevice environment, protein-rich environment with and without inflammatory conditions). When the protective surface oxide (passive film) was disrupted through the friction process (fretting), all samples started to corrode at an equilibrium between repassivation and depassivation (repeatedly reforming and destroying the passive film). The presence of 30 mM H_2O_2 accelerated the passivation process and resulted hence in the narrowest wear track. The activation of the surface was strongest in the presence of the proteins (BSA) without any H_2O_2, probably due to a hindrance of repas-

sivation due to adsorption of the BSA on cathodic sites. HCl resulted in a localized tribocorrosion process. The grain sizes were smaller and the microhardness higher for AM than forged samples. There was no influence of the manufacturing process on the COF in HCl and PBS+BSA solutions, however, a significantly higher COF was found for forged samples in PBS+BSA+H_2O_2 than AM samples, probably due to different wear debris. Also, forged samples had a larger wear track and showed signs of more corrosion in all solutions.

Data availability statement

The raw data for the figures of this study are openly available in OSF at https://osf.io/4nx2d/.

Funding

Declaration of Competing Interest

The authors declare that they have no known competing financial interests or personal relationships that could have appeared to influence the work reported in this paper.

Data availability

Data will be made available on request.

Supplementary materials

Supplementary material associated with this article can be found, in the online version, at doi:10.1016/j.addlet.2023.100156.

References

[1] J.L. Gilbert, Corrosion in the human body: metallic implants in the complex body environment, Corrosion 73 (12) (2017) 1478–1495.

[2] L. Zhou, T. Yuan, J. Tang, J. He, R. Li, Mechanical and corrosion behavior of titanium alloys additively manufactured by selective laser melting – A comparison between nearly β titanium, α titanium and $\alpha + \beta$ titanium, Opt. Laser Technol. 119 (2019) 105625.

[3] M. Abdel-Hady Gepreel, M. Niinomi, Biocompatibility of Ti-alloys for long-term implantation, J. Mech. Behav. Biomed. Mater. 20 (2013) 407–415.

[4] M. Prestat, D. Thierry, Corrosion of titanium under simulated inflammation conditions: clinical context and *in vitro* investigations, Acta Biomater. 136 (2021) 72–87.

[5] S. Ferraris, Y.S. Hedberg, J.J. Noël, S. Spriano, Interactions between the physiological environment and titanium-based implant materials: from understand-ing to control, in: Nanoscale Engineering of Biomaterials: Properties and Applications, Springer, 2022, pp. 3–26. https://link.springer.com/chapter/10.1007/978-981-16-3667-7_1.

[6] M. Kaur, K. Singh, Review on titanium and titanium based alloys as biomaterials for orthopaedic applications, Mater. Sci. Eng. C Mater. Biol. Appl. 102 (2019) 844–862.

[7] N. Eliaz, Corrosion of metallic biomaterials: a review, Materials (Basel) 12 (3) (2019) 407.

[8] E. Rezvani Ghomi, F. Khosravi, R.E. Neisiany, S. Singh, S. Ramakrishna, Future of additive manufacturing in healthcare, Curr. Opin. Biomed. Eng. 17 (2021) 100255.

[9] M.H. Shahini, H.E. Mohammadloo, B. Ramezanzadeh, Recent approaches to limit the tribocorrosion of biomaterials: a review, Biomass Convers. Biorefinery (2022), doi:10.1007/s13399-022-02719-3.

[10] S. Carquigny, J. Takadoum, S. Ivanescu, Corrosion and tribocorrosion study of 316L steel, Ti–6Al–4V and Ti–10Zr–10Nb–5Ta, Tribol. Mater. Surf. Interfaces 13 (2) (2019) 112–119.

[11] J. Villanueva, L. Trino, J. Thomas, D. Bijukumar, D. Royhman, M.M. Stack, M.T. Mathew, Corrosion, tribology, and tribocorrosion research in biomedical implants: progressive trend in the published literature, J. Bio Tribo Corros. 3 (2017) 1.

[12] M.J. Runa, M.T. Mathew, L.A. Rocha, Tribocorrosion response of the Ti6Al4V alloys commonly used in femoral stems, Tribol. Int. 68 (2013) 85–93.

[13] V. Gopal, G. Manivasagam, Wear – Corrosion synergistic effect on Ti–6Al–4V alloy in H_2O_2 and albumin environment, J. Alloys Compd. 830 (2020) 154539.

[14] E. Liamas, O.R.T. Thomas, A.I. Munoz, Z.J. Zhang, Tribocorrosion behaviour of pure titanium in bovine serum albumin solution: a multiscale study, J. Mech. Behav. Biomed. Mater. 102 (2020) 103511.

[15] S. Pal, G. Lojen, V. Kokol, I. Drstvensek, Evolution of metallurgical properties of Ti-6Al-4V alloy fabricated in different energy densities in the selective laser melting technique, J. Manuf. Process. 35 (2018) 538–546.

[16] M. Yakout, M.A. Elbestawi, S.C. Veldhuis, A study of the relationship between thermal expansion and residual stresses in selective laser melting of Ti-6Al-4V, J. Manuf. Process. 52 (2020) 181–192.

[17] Y.S. Hedberg, M. Znidarsic, G. Herting, I. Milosev, I. Odnevall Wallinder, Mechanistic insight on the combined effect of albumin and hydrogen peroxide on surface oxide composition and extent of metal release from Ti6Al4V, J. Biomed. Mater. Res. B Appl. Biomater. 107 (3) (2019) 858–867.

[18] S.A. Mali, Mechanically assisted crevice corrosion in metallic biomaterials: a review, Mater. Technol. 31 (12) (2016) 732–739.

[19] A. Manoj, A.K. Kasar, P.L. Menezes, Tribocorrosion of porous titanium used in biomedical applications, J. Bio- Tribo-Corros. 5 (2019) 3.

[20] M. Buciumeanu, A. Araujo, O. Carvalho, G. Miranda, J.C.M. Souza, F.S. Silva, B. Henriques, Study of the tribocorrosion behaviour of Ti6Al4V – HA biocomposites, Tribol. Int. 107 (2017) 77–84.

[21] F. Yu, O. Addison, A.J. Davenport, A synergistic effect of albumin and H_2O_2 accelerates corrosion of Ti6Al4V, Acta Biomater. 26 (2015) 355–365.

[22] Y. Zhang, O. Addison, F. Yu, B.C.R. Troconis, J.R. Scully, A.J. Davenport, Time-dependent enhanced corrosion of Ti6Al4V in the presence of H_2O_2 and albumin, Sci. Rep. 8 (1) (2018) 3185.

[23] Y.S. Hedberg, F. Gamna, G. Padoan, S. Ferraris, M. Cazzola, G. Herting, M. Atapour, S. Spriano, I. Odnevall Wallinder, Surface modified Ti6Al4V for enhanced bone bonding ability – effects of silver and corrosivity at simulated physiological conditions from a corrosion and metal release perspective, Corros. Sci. 168 (2020) 108566.

[24] S. Kumar, T.S.N.S. Narayanan, S. Ganesh Sundara Raman, S.K. Seshadri, Surface modification of CP-Ti to improve the fretting-corrosion resistance: thermal oxidation vs. anodizing, Mater. Sci. Eng. C 30 (6) (2010) 921–927.

[25] G. Chi, D. Yi, H. Liu, Effect of roughness on electrochemical and pitting corrosion of Ti-6Al-4V alloy in 12wt.% HCl solution at 35 °C, J. Mater. Res. Technol. 9 (2) (2020) 1162–1174.

[26] A. Kumar, K. Biswas, B. Basu, Fretting wear behaviour of hydroxyapatite–titanium composites in simulated body fluid, supplemented with 5g l−1 bovine serum albumin, J. Phys. D Appl. Phys. 46 (40) (2013) 404004.